Organic–inorganic hybrid materials for interface design in all-solid-state batteries with garnet-type solid electrolyte

Nataly Carolina Rosero-Navarro,[*a] Ryunosuke Kajiura,[b] Akira Miura,[a] and Kiyoharu Tadanaga*[a]

[a.] *Division of Applied Chemistry, Faculty of Engineering, Hokkaido University, Sapporo 060-8628, Japan*

[b.] *Graduate School of Chemical Sciences and Engineering, Hokkaido University, Sapporo 060-8628, Japan*

* E-mail address: rosero@eng.hokudai.ac.jp, tadanaga@eng.hokudai.ac.jp

Abstract

The practical realization of all-solid-state lithium-metal batteries depends on the development of low interfacial resistance between the solid electrolyte and electrodes. Herein, an organic–inorganic hybrid solid electrolyte, formed by an organic network of poly(ethylene oxide) chains that is connected with an inorganic Si–O–Si backbone network containing lithium salt, is proposed as a new interfacial material between a garnet-type oxide solid electrolyte and high-potential cathodes. The properties of the hybrid solid electrolyte are evaluated to obtain a material that is chemically and electrochemically compatible with the solid electrolyte and active material. Thereafter, the different procedures to fabricate a low-resistance solid–solid interface between the solid electrolyte and $LiCoO_2$ using the hybrid solid electrolyte are evaluated. The hybrid solid electrolyte provides an ionic/electronic percolation of active material particles and excellent adherence properties, thereby enabling the operation of the all-solid-state battery at room temperature to achieve a high initial discharge capacity of 125 $mAh.g^{-1}$.

Keywords: garnet-type solid electrolyte, all-solid-state battery, cathode-electrolyte interface, hybrid solid electrolyte, interfacial layer, solid-solid interfaces

1. Introduction

The realization of all-solid-state lithium-metal batteries has been actively investigated because of their potential to deliver the higher energy density and safety required for energy storage in large-scale applications. The wide electrochemical window of the oxide solid electrolytes with garnet structure (e.g., $Li_7La_3Zr_2O_{12}$, LLZ) presents the possibility to combine it with high-potential electrodes and lithium metal. The interfacial resistance between the solid electrolyte and electrodes has been a "trending topic" over the last few years, especially considering that it is the key factor that determines the transport properties in batteries.[1-2] Two types of interfaces have been studied to reduce interfacial electrode–electrolyte resistance: solid–liquid and solid–solid interfaces. The solid-liquid interfaces refer to the addition of conventional liquid electrolytes based on lithium salts and organic solvents, including ionic liquid electrolytes, to reduce the interfacial resistance between the solid electrolyte and lithium metal or cathode composite electrodes (CEs) (Li | garnet and cathode | garnet interfaces hereafter). The liquid electrolyte can easily wet the surfaces of the solid electrolyte and electrodes, thereby increasing the contact area between them, which results in a low-resistance solid–liquid interface. Although these quasi-solid-state batteries can operate at room temperature with a reasonable current density,[1] the use of liquid electrolytes seems impractical from the application or commercialization perspective. Furthermore, the limitation of liquid electrolytes based on their electrochemical window and safety issues remains. On the other hand, the solid–solid interfaces refer to the absence of liquid phases at the interface. The development of solid–solid interfaces has gradually progressed; whereby different approaches have been presented for the lithium metal and composite cathode sides.

For the Li | garnet solid–solid interfaces, the use of buffer coating layers, such as Al_2O_3, Si, ZnO_2, and Au, as well as Li-alloys have allowed the achievement of solid–solid interfaces with significative low interfacial resistances.[2] Conversely, the cathode | garnet solid–solid interface is still a challenge. The direct deposition of the active material or the use of CEs has been evaluated to create cathode | garnet solid–solid ceramic (oxide-type linkage) interfaces with low resistance. The pulsed laser deposition (PLD) process[3-6] has been used to prepare dense cathode material (e.g., $LiCoO_2$) layers on the garnet solid electrolyte, while the co-sintering[7-8] or screen-printing[9-13] process has been employed in the application of CEs on the solid electrolyte surface. CEs include active materials, solid electrolytes as ionic conductor additives, as well as electronic conductor additives (e.g., In_2O_5Sn and carbon) and/or inorganic binders (e.g., Li_3BO_3 and Li_2SiO_3) to ensure particle percolation through the composite. The high reactivity of the garnet-type solid electrolyte is a common problem in the evaluated strategies to create ceramic solid–solid interfaces. Unfavorable reactions at the interface, such as the formation of Li_2CO_3 or $LaCoO_2$, are promoted by PLD or high co-sintering temperatures, and porosity remains a cause of the deficient sintering. Moreover, the rigid nature of this type of interface apparently produces additional defects, such as cracks or voids, through the CE during charge–discharge processes, thereby resulting in a loss of ionic and electronic contacts, which inevitably leads to capacity fade.

Consequently, a solid–solid interface, using polymeric materials, can be a feasible alternative that exhibits improved mechanical properties to enhance the interfacial cathode | garnet resistance, as well as to compensate for strain issues during battery operations. Du et al.[14] reported, for the first time, a solid–solid interface using a polymer to reduce the cathode

| garnet interfacial resistance, wherein a CE containing $LiFePO_4$ as the active material supported in a poly(vinylidene fluoride) polymeric matrix and $Li(CF_3SO_2)_2N$ (LiTFSI) as the Li-ion conductor additive were used. In contrast to ceramic solid–solid interfaces, CE is supported in a polymeric matrix that does not contain a solid electrolyte; therefore, the energy density of the battery is also expected to be improved with better utilization of the active material. A poly(ethylene oxide) (PEO)-based polymer with LiTFSI has also been used as an interfacial layer to reduce the interfacial cathode | garnet resistance[15]. These all-solid-state lithium metal batteries are operated at relative high temperatures of approximately 60–100 °C because of the limited conductivity through the polymeric interface. Further improvements in the interfacial resistance of these solid–solid interfaces using polymeric materials are achievable only with the addition of liquid electrolytes, whereby the battery can be operated at room temperature.[1, 16-17] In this study, a new solid–solid interface for cathode | garnet-type oxide solid electrolyte interface is designed toward developing an all-solid-state lithium-metal battery that can achieve not only high capacities but also can be operated at room temperature (25 °C). The battery consists of the Al-doped $Li_{6.75}La_{2.75}Ca_{0.25}Zr_{1.5}Ta_{0.5}O_{12}$ (LLCZT) solid electrolyte, $LiCoO_2$ as the cathode, and lithium metal as the anode. The interfacial material is based on a hybrid solid electrolyte, as illustrated in Figure 1.

This organic–inorganic hybrid material is formed by a crosslinked organic and inorganic structure mixed at the molecular level (hybrid class type II) [18-19]; an organic component formed by PEO chains covalent bonded with an inorganic component formed by the Si–O–Si backbone containing lithium salt. In contrast to PEO-based polymers, the inorganic component formed by the Si–O–Si backbone is expected to increase the random distribution

of PEO channels, which therefore, increases ionic conductivity at room temperature.[19-25] The properties of the hybrid solid electrolyte are evaluated to obtain a material that is chemically and electrochemically compatible with the solid garnet electrolyte and cathode active material. Thereafter, different procedures to fabricate a low-resistance solid–solid interface between LLCZT and the cathode active material by using a hybrid solid electrolyte are evaluated. The hybrid solid electrolyte acts as unique binder material that promotes the percolation of cathode active material particles in flexible supports with sufficient ionic conductivity by the organic chains present in the hybrid structure, thereby providing excellent adherence at the electrode/electrolyte interface owing to its silica-rich domains that allow the operation of an all-solid-state battery at room temperature, while achieving a high initial discharge capacity of 125 $mAh.g^{-1}$.

2. Results and discussion

2.1 Properties of the hybrid solid electrolyte

The hybrid material was prepared via a soft chemistry route using ethylene glycol diglycidyl ether (EGDE) and 3-glycidoxypropyltrimethoxy silane (GPTMS) as precursors (Figure 1). The hybrid precursor solution is obtained from the polymerization of epoxy-ring groups (blue circle in Figure 1), as well as the hydrolysis and polycondensation of silica species (green circle in Figure 1) at 60 °C. Two lithium sources—lithium perchlorate ($LiClO_4$) and LiTFSI—are evaluated to promote lithium conductivity through the organic–inorganic network. Figure 2a shows photographs of the hybrid precursor solution containing

$LiClO_4$ and derived membrane prepared by casting and subsequent heat treatment at temperatures between 60–120 °C (details are provided in the experimental section of the supporting information). The hybrid precursor solution is colorless, and the addition of lithium sources does not significantly change its appearance. Hybrid solid electrolytes with thickness values between 500–800 μm are slightly yellow, transparent, and homogeneous with suitable mechanical strength. The lithium-free hybrid membranes displayed the same characteristics, thereby suggesting that the incorporation of lithium salts does not produce appreciable changes. The absence of precipitates or aggregates on the cross-sectional surface of the membrane was verified by high-resolution scanning electron microscopy (SEM) observation (Figure S1), while the crosslinked organic–inorganic network structure was verified by means of Fourier-transform infrared spectroscopy (FTIR). Figure S2 shows the FTIR spectra of hybrid solid electrolytes prepared with $LiClO_4$ and LiTFSI. The FTIR spectra reveal similar bands in good agreement with other polymer electrolytes with comparable compositions. The polymerization and polycondensation reactions were confirmed by the presence of the stretching vibration of Si–O–C (1050 cm^{-1}) and the asymmetric vibration of Si–O–Si (1094 cm^{-1}).[21, 26]

Furthermore, the absence of absorption peaks at 1260 cm^{-1} (breathing vibration) and 912 cm^{-1} (symmetric stretching vibration)[21] indicates that the epoxy group is polymerized. For the LiFTSI-containing hybrid solid electrolyte, the absorption peaks at 1400–1100 cm^{-1} are associated with $TFSI^-$ anion.[21]

Figures 2b–g show the electrochemical characterization of hybrid solid electrolytes, comparing the effects of the lithium source ($LiClO_4$ and LiTFSI). The impedance spectra of

hybrid solid electrolytes (Figure 2b) at room temperature exhibit a semicircle at high frequencies with its center at approximately 10^5 Hz, whereas its tail is at low frequencies (10^3–10^4 Hz and c.a. 1 Hz). The semicircle is associated to the total resistance of the sample, while the capacitive tail is attributed to the diffusion behavior at the interface between the hybrid solid electrolytes and the current electrodes. The resistances of hybrid solid electrolytes were extracted by data fitting to equivalent circuits (Figure S5a). The total conductivity at room temperature of hybrid solid electrolytes containing $LiClO_4$ and LiTFSI, derived from total resistance and geometrical parameters of the membranes, are 1.6×10^{-5} $S.cm^{-1}$ and 2.0×10^{-5} $S.cm^{-1}$, respectively. Figure 2c shows the temperature dependence of the total lithium-ion conductivity of the hybrid solid electrolytes in the temperature range between 27–100 °C. The activation energies, derived from the Arrhenius equation, are 0.36 eV and 0.47 eV for the hybrid solid electrolyte containing $LiClO_4$ and LiTFSI, respectively. Figures 2d–g show the cyclic voltammogram (CV) of hybrid solid electrolytes containing $LiClO_4$ and LiTFSI at 25 °C and 60 °C. The CV at room temperature of hybrid solid electrolyte containing $LiClO_4$ (Figure 2d) does not show redox peaks in the range of 0–5 V, remaining rather stable in the wide electrochemical window, while the CV at 60 °C (Figure 2e) exhibits an oxidation peak at approximately 3.9 V, which is attributed to the decomposition reaction of PEO chains.[27] However, the CV of the hybrid solid electrolyte containing LiTFSI (Figures 2f and 2g) at room temperature and 60 °C indicates negligible redox reactions. The peak approximately at 2.5 V of the CV at room temperature is not assigned to the redox behavior of the hybrid solid electrolyte but is attributable to the oxidation of impurities (e.g. uncondensed silanol groups) on the surface of the organic–

inorganic hybrid membrane.[19, 28] The electrochemical properties of hybrid solid electrolytes coincide with other polymer electrolytes with similar composition.[19, 21, 25]

The ionic conduction mechanism of both hybrid solid electrolytes, consisting of both cation (Li^+) and anion ($TFSI^-$, ClO_4^-) carriers through the PEO structure, seems to be similar at room temperature. However, at higher temperatures, the slight improvement in the electrochemical properties of the LiTFSI-containing hybrid solid electrolyte is associated to its anion contribution. Notably, larger TFSI- anions can easily dissociate in the PEO matrix and set off the free lithium cations, thereby resulting in an increase in ionic conductivity. Moreover, the high flexibility of the $–SO_2–N–SO_2–$ of TFSI and a strong electron-withdrawing group ($SO_2–CF_3$) are the reasons for the electrochemical stability at high temperatures.[20] Both hybrid solid electrolytes containing $LiClO_4$ or LiTFSI exhibit a wide potential window of 0–5 V at 25 °C, making them compatible with garnet-type oxide solid electrolytes and high-potential cathodes. An ionic conductivity of approximately 10^{-5} $S.cm^{-1}$ is expected to further provide sufficient ionic conductivity in the composite electrode.

2.2 All-solid-state battery by using a composite electrode

Two different procedures are investigated to prepare a low-resistance solid–solid interface between LLCZT and the cathode active material by using the hybrid solid electrolyte. The first is the fabrication of the all-solid-state battery named as Li/LS/LLCZT/LS/CE-hybrid ($LiClO_4$ or LiTFSI) (Section 2.2.1), wherein the CE, containing $LiCoO_2$ and hybrid solid electrolyte, is obtained via a screen-printing process. The second is Li/LS/LLCZT/LS/CES-hybrid (LiTFSI) obtained by means of a self-supported composite

electrode sheet (CES) obtained through a doctor-blade method (Section 2.2.2). LS represent the lithium silicate buffer layer. Notably, for the lithium-side interface, the LLCZT pellet was previously coated with LS buffer layer to obtain low interfacial resistance according to a previously described procedure.[29] All-solid-state batteries are operable, demonstrating the effectiveness of the hybrid solid electrolyte as an interfacial material. Parameters that affect the electrochemical performance properties of all-solid-state batteries based on the fabrication process are elucidated by comparing these two procedures. Table I summarize the configuration of all-solid-state batteries prepared with composite electrode using hybrid solid electrolytes.

2.2.1 All-solid-state battery by using a composite electrode obtained by the screen-printing process

Figure 3a presents an illustration of the fabrication of the all-solid-state battery by screen-printing of the composite electrode. First, a CE slurry containing the precursor solution of the hybrid solid electrolyte and $LiCoO_2$ is prepared. Carbon is also used as an electronic additive; however, it is not illustrated to facilitate the explanation. Second, the slurry is directly dropped on the surface of the LLCZT pellet. Finally, and after heat treatment to consolidate the CE layer, the all-solid-state battery is assembled using lithium metal on the free-side of the LLCZT pellet and stainless steel (SS) current collectors. The chemical compatibility between the hybrid solid electrolyte with $LiCoO_2$ and the solid electrolyte was studied via X-ray diffraction (XRD). The absence of secondary phases and rather unchanged XRD patterns of $LiCoO_2$ and LLCZT-containing hybrid solid electrolyte (Figure S3)

compared with their respective reference XRD patterns suggest that neither the hybrid material nor heat treatment produces unfavorable reactions. Figures 3b and 3c–e show high resolution images of $LiCoO_2$ particles and CE -containing hybrid solid electrolyte with $LiClO_4$ salt obtained via SEM, respectively. The $LiCoO_2$ particles have a regular distribution with an average size of approximately 200 nm. The surface of the CE (Figure 3c) is smooth, corresponding to the hybrid solid electrolyte, wherein the morphology of the $LiCoO_2$ particles is recognizable. The higher magnification of the CE (Figure 3d) displays particle agglomeration not higher than 1 μm, which is well connected by the hybrid solid electrolyte between them. The voids observed in the figure were created during the SEM observation by beam exposure at high resolution. The cross section of the interface between the CE and LLCZT (Figure 3e) shows a well-adhered layer of the CE along the surface of the LLCZT pellets, thereby suggesting sufficient physical solid–solid contact at the electrode/electrolyte interface, which is facilitated by the hybrid solid electrolyte. The solid–solid contacts are created using a precursor solution of the hybrid material that is easily wettable and penetrates the solid particles of the active material, whereafter the consolidation of the hybrid material with heat treatment at approximately 120 °C maintains a continued layer with sufficient contact between the electrode and electrolyte without unfavorable reactions.

Figures 3f–g and 3h–i show the impedance profiles of as-prepared all-solid-state batteries and initial charge–discharge profiles using CEs with a hybrid solid electrolyte containing $LiClO_4$ and LiTFSI, respectively. Surprisingly, the batteries showed a high internal resistance at room temperature, exceeding the detection limit of the impedance analyzer; therefore, the batteries were heated at 60 °C to perform the electrochemical characterization. The

impedance profile of the Li/LS/LLCZT/CE-hybrid ($LiClO_4$) cell (Figure 3f, top) shows non-symmetric overlapping semicircles, achieving a total resistance of approximately 21 $k\Omega \cdot cm^2$ at ~0.01 Hz (Figure S5), wherein the depletion of the semicircle is observed. The impedance profile of the Li/LS/LLCZT/LS/CE-hybrid ($LiClO_4$) cell (Figure 3f, bottom), wherein the lithium silicate buffer layer is used as an interfacial layer between solid electrolyte and CE, shows overlapping semicircles at high frequencies with a total resistance of approximately 2.4 $k\Omega \cdot cm^2$ at ~1 Hz (Figure S5), followed by the typical tail at low frequencies corresponding to solid-state ion diffusion into active material ($LiCoO_2$). The impedance profile of the Li/LS/LLCZT/LS/CE-hybrid (LiTFSI) cell (Figure 3g) shows a similar profile to that obtained from the Li/LS/LLCZT/LS/CE-hybrid ($LiClO_4$) cell, with a semicircle at high frequencies achieving a total resistance of approximately 2.4 $k\Omega \cdot cm^2$ at ~10 Hz (Figure S5), followed by the tail at low frequencies. Both the wide and overlapping semicircles at high frequencies observed in the Li//LS/LLCZT/CE-hybrid ($LiClO_4$), Li/LS/LLCZT/LS/CE-hybrid ($LiClO_4$), and Li/LS/LLCZT/LS/CE-hybrid (LiTFSI) cells should contain the combination of similar resistance contributions, including LLCZT solid electrolyte resistance, LLCZT/Li, LLCZT/LS, and LLCZT/CE-hybrid interfacial resistances, as well as interfacial resistances through the CE between $LiCoO_2$ and the hybrid solid electrolyte. The resistance of the solid electrolyte and the interfacial resistance with lithium metal by using lithium silicate (Li/LS/LLCZT) is estimated to achieve ~0.5 $k\Omega \cdot cm^2$.[29] This resistance can be subtracted to the total resistance of the batteries to estimate the resistance contribution corresponding to the cathode side. Thus, the interfacial resistance of the solid electrolyte with and through the CE (ionic resistance of hybrid solid electrolyte) can be estimated to be 16

$k\Omega \cdot cm^2$ for the Li/LS/LLCZT/CE-hybrid ($LiClO_4$) cell, as well as ~1.9 $k\Omega \cdot cm^2$ for the Li/LS/LLCZT/LS/CE-hybrid ($LiClO_4$) and Li/LS/LLCZT/LS/CE-hybrid (LiTFSI) cells. Figures 3h and 3i show the initial charge–discharge profiles of the Li/LS/LLCZT/CE-hybrid ($LiClO_4$), Li/LS/LLCZT/LS/CE-hybrid ($LiClO_4$), and Li/LS/LLCZT/LS/CE-hybrid (LiTFSI) cells at 60 °C. The initial discharge capacities attain 45 $mAh.g^{-1}$, 58 $mAh.g^{-1}$ and 98 $mAh.g^{-1}$, with a coulombic efficiency of 33%, 45%, and 75% for the Li/LS/LLCZT/CE-hybrid ($LiClO_4$), Li/LS/LLCZT/LS/CE-hybrid ($LiClO_4$), and Li/LS/LLCZT/LS/CE-hybrid (LiTFSI) cells, respectively.

The impedance profiles reveal that using the lithium silicate buffer layer dramatically decreases the interfacial resistance between the solid electrolyte and CE, resulting in a drop in the total internal battery resistance by more than 1 order of magnitude. The difference between the lithium silicate buffer layer and the hybrid solid electrolyte is associated to the different wettability properties. The lithium silicate buffer layer has proven to considerably improve the interfacial resistance with the lithium metal[29] and $LiNi_{1/3}Mn_{1/3}Co_{1/3}O_2$ active material,[13] thanks to its wettability properties. For the hybrid material, the polymeric phase of hybrid matrix could produce hydrophobic regions compared with the complete inorganic lithium silicate network; therefore, the presence of the lithium silicate buffer layer improved effectively the connectivity between solid electrolyte and hybrid material. The inorganic phase (-Si-O-Si-) of the hybrid matrix may strengthen this chemical affinity resulting in this effective adherence. On the other hand, the symmetry of the semicircles at high frequencies of the Li/LS/LLCZT/LS/CE-hybrid ($LiClO_4$) and Li/LS/LLCZT/LS/CE-hybrid (LiTFSI) cells suggests that the individual contribution of different associated resistance values is

different; however, the total internal battery resistances achieve the same value, which indicates that the lithium source in the hybrid solid electrolyte is rather negligible. However, the effect of the lithium salt in the hybrid solid electrolyte on battery performance is notably different. The high initial discharge capacity is achieved by the battery using the hybrid solid electrolyte with LiTFSI salt, which is attributed to its stable and wide electrochemical window at 60 °C (Figure 2g).

Although the battery can achieve a reasonable initial discharge capacity, which indicates that the hybrid solid electrolyte acts effectively as a buffering layer between active material particles allowing ionic and electronic percolation through the CE and solid electrolyte, the electrochemical performance at room temperature remains poor. The absence of secondary phases and the apparent sufficient physical contact between the solid electrolyte and CE verified by XRD and SEM analyses do not provide clear evidence toward understanding the reason for this behavior. A possible reason could be local reactions at the interface promoted by the in situ deposition of the CE slurry. The presence of several phases, such as La_2O_3, $La_2Zr_2O_7$, $Li_6Zr_2O_7$, Li_2CoO_3, and Li_5CoO_4, determined through first-principles calculations at the $Li_{1-x}CoO_2$/LLZ electrochemical interface,[30] can also be a reason of the limited electrochemical behavior. However, the local presence of these phases at the interface is difficult to detect via XRD.[30]

2.2.2 All-solid-state battery by using a self-supported composite electrode sheet

Figure 4a shows an illustration of the fabrication of the all-solid-state battery using a self-supported CES to prevent the direct contact of the solution precursor of the hybrid solid

electrolyte with the LLCZT pellet. First, a slurry of the composite electrode containing hybrid solid electrolyte, $LiCoO_2$, and carbon is deposited on the aluminum foil by the doctor-blade method. Second, the CES is obtained after heat treatment at 100 °C, leading to the consolidation of the composite electrode. Finally, the all-solid-state battery is assembled using lithium metal, CES, LLCZT pellet, and SS current collectors. The LLCZT pellet was coated previously with lithium silicate buffer layer on both pellet faces to facilitate interfacial resistance. Figure 4b shows the appearance of the lithium metal, CES, and LLCZT pellet before battery assembly. The physical contact of the LLCZT pellet with lithium metal and CES is obtained by a simple pressing procedure. The hybrid solid electrolyte with LiTFSI was used as CES electrolyte, and the effect of $LiCoO_2$ particle size on the electrochemical performance of the battery was evaluated. The all-solid-state batteries are named Li/LS/LLCZT/LS/CES-hybrid (LiTFSI). The composite electrode sheet was prepared with two different particle sizes of $LiCoO_2$ with sizes of approximately 200 nm (small LCO) and 2 μm (big LCO). Figures 4c–d show the SEM images of the surface and cross section of the CES-hybrid (LiTFSI) with small and big LCO, respectively. The surface of both CESs is smooth for the hybrid solid electrolyte and the $LiCoO_2$, and the carbon particles embedded in the hybrid polymeric matrix with a high homogeneity distribution were also verified in low-resolution images (Figure S4). SEM-EDS analysis of the cross section of the CES-hybrid (LiTFSI) with small and big LCO also confirm the percolation of the $LiCoO_2$ particles through the hybrid solid electrolyte. Voids are created during the cross-sectional preparation by the focused ion beam.

Figures 4g-h and 4i–j show impedance profiles and initial charge–discharge profiles of the Li/LS/LLCZT/LS/CES-hybrid (LiTFSI) cells with small and big LCO at 25 °C. The impedance profile of Li/LS/LLCZT/LS/CES- hybrid with small and big LCO cells are similar to those obtained from the Li/LS/LLCZT/LS/CE-hybrid (LiTFSI) cell (Figure 3g) with a non-symmetric semicircle at high frequencies, achieving a total resistance of approximately ~2.5 kΩ·cm^2 and ~1.8 kΩ·cm^2 at ~10 Hz (Figure S5), followed by the tail at low frequencies, respectively. Considering the lithium metal interface by the lithium silicate layer (~0.5 kΩ·cm^2),[29] the interfacial resistance values with and through the composite electrode are estimated to be ~2.0 kΩ·cm^2 and ~1.3 kΩ·cm^2 for the Li/LS/LLCZT/LS/CES-hybrid (LiTFSI) cells with small and big LCO, respectively. The impedance profile of Li/LS/LLCZT/CES-hybrid (LiTFSI) cell, without lithium silicate buffer layer in the cathode side (Figure S6), displays a total resistance of approximately ~70 kΩ·cm^2 which is higher than 1 order of magnitude of the batteries using LLCZT/LS/CES interface. The initial discharge capacities were 60 mAh.g^{-1} and 125 mAh.g^{-1}, with coulombic efficiencies of 75% and 84% for the Li/LS/LLCZT/LS/CES-hybrid (LiTFSI) cells with small and big LCO, respectively.

The total resistance of the Li/LS/LLCZT/LS/CE-hybrid (LiTFSI) (Figure 3g) and Li/LS/LLCZT/LS/CES-hybrid (LiTFSI) with small LCO (Figure 4g) cells achieves a similar value ~2.5 kΩ·cm^2, thereby suggesting that the internal resistance of the batteries and their components are considerably unaffected by the fabrication procedure between the direct application of the CE on the surface of the solid electrolyte nor by the use of CES. However, the charge–discharge curves of the Li/LS/LLCZT/LS/CES- hybrid (LiTFSI) cell with small

LCO (Figure 4i) show a low ohmic drop with a stable Co^{3+}/Co^{4+} redox plateau at 4.0 V/3.8 V, indicating that the lithium intercalation process is conducted easily through the interface, even if the total initial discharge capacity is less than that of the Li/LS/LLCZT/LS/CE-hybrid (LiTFSI) cell (Figure 3i). However, the use of composite electrodes with bigger $LiCoO_2$ particle sizes seems to improve the internal resistance of the battery (~1.3 $k\Omega \cdot cm^2$) because of the reduction of the surface area; therefore, the interfacial contacts between the $LiCoO_2$ and hybrid solid electrolyte marginally contribute to the improvement of the initial discharge capacity up to 125 $mAh.g^{-1}$. In addition, the lithium silicate buffer layer has been found to be essential to achieve the low interfacial resistance of the all-solid-state battery at room temperature. Therefore, using the CES containing the hybrid solid electrolyte combined with surface modification of solid electrolyte leads to a low interfacial resistance by a simple procedure at room temperature, thereby overcoming one of the major challenges in the field of all-solid-state batteries based on garnet-type oxide solid electrolytes because of its rigid nature. Moreover, this procedure is particularly attractive for further industrial applications, wherein the all-solid-state battery can be obtained by a simple press procedure on their components.

2.3 Current status and perspectives

Table II summarizes the initial discharge capacity of all-solid-state lithium-metal batteries based on garnet-type oxide solid electrolytes prepared by different strategies to reduce cathode | garnet solid–solid interfacial resistance using solid–solid interfaces. Taking the $LiCoO_2$ electrode as a reference, the initial discharge capacity can vary from 125–78

$mAh.g^{-1}$ for ceramic solid–solid interfaces. The highest initial discharge capacity is reported for all-solid-state batteries wherein the active material is deposited by PLD because of the better and intimate contact between the solid electrolyte and active material. For the solid–solid interfaces using polymers, the initial discharge capacity is comparable to those obtained by PLD in terms of the relation between practical and theoretical capacities, achieving ~80%.

The designed organic–inorganic hybrid solid–solid interface used in this study is comparable to both the solid–solid interfaces (ceramic or using polymers), which is beneficially obtained by a simple process at low temperature and is operable at room temperature. It is also envisaged that this type of self-supported electrodes using a hybrid solid electrolyte are adaptable to other solid electrolytes and active materials; therefore, the development of all-solid-state batteries with different properties is anticipated.

Conclusions

A cathode | garnet solid–solid interface, based on an organic–inorganic hybrid solid electrolyte formed by a crosslinked poly(ethylene oxide) chain structure with Si–O–Si backbones and containing lithium salt, was developed. Hybrid solid electrolytes containing $LiClO_4$ or LiTFSI salts show ionic conductivities of approximately 10^{-5} $S.cm^{-1}$, with a wide electrochemical potential window up to 5 V at room temperature, making them compatible with garnet-type oxide solid electrolyte and high-potential cathodes. Two different procedures were investigated to prepare a low-resistance solid–solid interface between the LLCZT solid electrolyte and $LiCoO_2$ active material by means of the hybrid solid electrolyte.

Notably, CEs containing cathode active material, carbon, and hybrid solid electrolytes, were prepared by screen-printing on the surface of the LLCZT solid electrolyte, as well as by using a self-supported CES. The hybrid solid electrolyte proves to be effective as interfacial material, acting as a unique binder material that promotes the percolation of cathode active material particles in a flexible support with sufficient ionic conductivity based on the organic chains present in the hybrid structure. Moreover, the silica-rich domains enhance the wettability of the solid electrolyte, providing for strong linkage between the solid electrolyte and cathode active material particles. The all-solid-state battery fabricated with the CES, LLCZT solid electrolyte, as well as lithium metal and assembled by a simple pressure procedure attains a high capacity of 125 $mAh.g^{-1}$ at room temperature, overcoming one of the major challenges in the field of all-solid-state batteries based on ceramic solid electrolytes.

Author Contributions

Conceptualization, N.C.R-N. and K.T.; Methodology, R.K., N.C.R-N. A.M. and K.T.; Investigation (experimental work), R.K. and N.C.R-N.; Writing – Original Draft, R.K. and N.C.R-N.; Writing – Review & Editing, N.C.R-N. A.M. and K.T.; Supervision, N.C.R-N. A.M. and K.T.; Funding Acquisition , N.C.R-N.

Declaration of interests

The authors declare no competing interests.

Acknowledgements

N.C.R.-N. acknowledges the Japan Society for Promotion of Science (JSPS) for financial support of this work through the national project "Grants-in-Aid for Scientific Research (KAKENHI)" (2017–2020) with reference number 17K17559 and SOUSEI Support Program for Young Researchers in FY2020 of Hokkaido University. The analysis of SEM-FIB was carried out with JIB4600F at the "Joint-use Facilities: Laboratory of Nano-Micro Material Analysis", Hokkaido University, supported by "Material Analysis and Structure Analysis Open Unit (MASAOU)". The authors thank Prof. Nobuyuki Miyasaki from the Laboratory of Nano-Micro Material Analysis for his assistance with SEM-FIB analysis.

References

1. Samson, A. J.; Hofstetter, K.; Bag, S.; Thangadurai, V., A bird's-eye view of Li-stuffed garnet-type $Li_7La_3Zr_2O_{12}$ ceramic electrolytes for advanced all-solid-state Li batteries. *Energy & Environmental Science* **2019,** *12* (10), 2957-2975.

2. Wang, C.; Fu, K.; Kammampata, S. P.; McOwen, D. W.; Samson, A. J.; Zhang, L.; Hitz, G. T.; Nolan, A. M.; Wachsman, E. D.; Mo, Y.; Thangadurai, V.; Hu, L., Garnet-Type Solid-State Electrolytes: Materials, Interfaces, and Batteries. *Chem. Rev.* **2020,** *120* (10), 4257-4300.

3. Ohta, S.; Kobayashi, T.; Asaoka, T., High lithium ionic conductivity in the garnet-type oxide Li_{7-X} $La_3(Zr_{2-X}, Nb_X)O_{12}$ (X=0–2). *J. Power Sources* **2011,** *196* (6), 3342-3345.

4. Ohta, S.; Kobayashi, T.; Seki, J.; Asaoka, T., Electrochemical performance of an all-solid-state lithium ion battery with garnet-type oxide electrolyte. *J. Power Sources* **2012,** *202* (0), 332-335.

5. Matsuyama, T.; Takano, R.; Tadanaga, K.; Hayashi, A.; Tatsumisago, M., Fabrication of all-solid-state lithium secondary batteries with amorphous TiS_4 positive electrodes and $Li_7La_3Zr_2O_{12}$ solid electrolytes. *Solid State Ionics* **2016,** *285*, 122-125.

6. Kato, T.; Hamanaka, T.; Yamamoto, K.; Hirayama, T.; Sagane, F.; Motoyama, M.; Iriyama, Y., In-situ $Li_7La_3Zr_2O_{12}/LiCoO_2$ interface modification for advanced all-solid-state battery. *J. Power Sources* **2014,** *260*, 292-298.

7. Ohta, S.; Seki, J.; Yagi, Y.; Kihira, Y.; Tani, T.; Asaoka, T., Co-sinterable lithium garnet-type oxide electrolyte with cathode for all-solid-state lithium ion battery. *J. Power Sources* **2014,** *265* (0), 40-44.

8. Kotobuki, M.; Munakata, H.; Kanamura, K.; Sato, Y.; Yoshida, T., Compatibility of Li7La3Zr2O12 Solid Electrolyte to All-Solid-State Battery Using Li Metal Anode. *J. Electrochem. Soc.* **2010,** *157* (10), A1076-A1079.

9. Ohta, S.; Komagata, S.; Seki, J.; Saeki, T.; Morishita, S.; Asaoka, T., All-solid-state lithium ion battery using garnet-type oxide and Li_3BO_3 solid electrolytes fabricated by screen-printing. *J. Power Sources* **2013,** *238* (0), 53-56.

10. Liu, T.; Ren, Y.; Shen, Y.; Zhao, S.-X.; Lin, Y.; Nan, C.-W., Achieving high capacity in bulk-type solid-state lithium ion battery based on $Li_{6.75}La_3Zr_{1.75}Ta_{0.25}O_{12}$ electrolyte: Interfacial resistance. *J. Power Sources* **2016,** *324*, 349-357.

11. Jin, Y.; McGinn, P. J., Bulk solid state rechargeable lithium ion battery fabrication with Al-doped $Li_7La_3Zr_2O_{12}$ electrolyte and $Cu_{0.1}V_2O_5$ cathode. *Electrochimica Acta* **2013,** *89*, 407-412.

12. Han, F.; Yue, J.; Chen, C.; Zhao, N.; Fan, X.; Ma, Z.; Gao, T.; Wang, F.; Guo, X.; Wang, C., Interphase Engineering Enabled All-Ceramic Lithium Battery. *Joule* **2018,** *2* (3), 497-508.

13. Alexander, George V.; Rosero-Navarro, N. C.; Miura, A.; Tadanaga, K.; Murugan, R., Electrochemical performance of a garnet solid electrolyte based lithium metal battery with interface modification. *J. Mater. Chem. A.* **2018,** *6* (42), 21018-21028.

14. Du, F.; Zhao, N.; Li, Y.; Chen, C.; Liu, Z.; Guo, X., All solid state lithium batteries based on lamellar garnet-type ceramic electrolytes. *J. Power Sources* **2015,** *300*, 24-28.

15. Chi, S.-S.; Liu, Y.; Zhao, N.; Guo, X.; Nan, C.-W.; Fan, L.-Z., Solid polymer electrolyte soft interface layer with 3D lithium anode for all-solid-state lithium batteries. *Energy Storage Materials* **2019,** *17*, 309-316.

16. Huo, H.; Zhao, N.; Sun, J.; Du, F.; Li, Y.; Guo, X., Composite electrolytes of polyethylene oxides/garnets interfacially wetted by ionic liquid for room-temperature solid-state lithium battery. *J. Power Sources* **2017,** *372*, 1-7.

17. Xu, B.; Duan, H.; Liu, H.; Wang, C. A.; Zhong, S., Stabilization of Garnet/Liquid Electrolyte Interface Using Superbase Additives for Hybrid Li Batteries. *ACS Appl. Mater. Interfaces* **2017,** *9* (25), 21077-21082.

18. Gomez-Romero, P.; Sanchez, C., Hybrid Materials, Functional Applications. An Introduction. In *Functional Hybrid Materials*, Wiley-VCH Verlag GmbH & Co. KGaA: 2003; pp 1-14.

19. Wang, Q.; Zhang, H.; Cui, Z.; Zhou, Q.; Shangguan, X.; Tian, S.; Zhou, X.; Cui, G., Siloxane-based polymer electrolytes for solid-state lithium batteries. *Energy Storage Materials* **2019,** *23*, 466-490.

20. Xue, Z.; He, D.; Xie, X., Poly(ethylene oxide)-based electrolytes for lithium-ion batteries. *J. Mater. Chem. A.* **2015,** *3* (38), 19218-19253.

21. Vélez, J. F.; Aparicio, M.; Mosa, J., Covalent silica-PEO-LiTFSI hybrid solid electrolytes via sol-gel for Li-ion battery applications. *Electrochimica Acta* **2016,** *213*, 831-841.

22. Zhang, J.; Ma, C.; Liu, J.; Chen, L.; Pan, A.; Wei, W., Solid polymer electrolyte membranes based on organic/inorganic nanocomposites with star-shaped structure for high performance lithium ion battery. *J. Membr. Sci.* **2016,** *509*, 138-148.

23. Boaretto, N.; Horn, T.; Popall, M.; Sextl, G., Optimization of the transport and mechanical properties of polysiloxane/polyether hybrid polymer electrolytes. *Electrochimica Acta* **2017,** *241*, 477-486.

24. Nakano, S.; Piedrahita, C. R.; Onozuka, R.; Adachi, K.; Tsukahara, Y.; Pugh, C.; Kyu, T., Effect of Chain Architectures of Star-shaped Poly(ethylene glycol) Macromonomers on Enhancement of Thermal, Mechanical, and Electrochemical Performance of Polymer Electrolyte Membranes. *Chem. Lett.* **2018,** *47* (4), 587-590.

25. Zhang, J.; Ma, C.; Hou, H.; Li, X.; Chen, L.; Ivey, D. G.; Wei, W., A star-shaped solid composite electrolyte containing multifunctional moieties with enhanced electrochemical properties for all solid-state lithium batteries. *J. Membr. Sci.* **2018,** *552*, 107-114.

26. Stefanescu, M.; Stoia, M.; Stefanescu, O., Thermal and FT-IR study of the hybrid ethylene-glycol–silica matrix. *Journal of Sol-Gel Science and Technology* **2007,** *41* (1), 71-78.

27. Miyashiro, H.; Kobayashi, Y.; Seki, S.; Mita, Y.; Usami, A.; Nakayama, M.; Wakihara, M., Fabrication of All-Solid-State Lithium Polymer Secondary Batteries Using Al_2O_3-Coated $LiCoO_2$. *Chemistry of Materials* **2005,** *17* (23), 5603-5605.

28. Fujinami, T.; Mehta, M. A.; Sugie, K.; Mori, K., Molecular design of inorganic–organic hybrid polyelectrolytes to enhance lithium ion conductivity. *Electrochimica Acta* **2000,** *45* (8), 1181-1186.

29. Rosero-Navarro, N. C.; Kajiura, R.; Jalem, R.; Tateyama, Y.; Miura, A.; Tadanaga, K., Significant Reduction in the Interfacial Resistance of Garnet-Type Solid Electrolyte and Lithium Metal by a Thick Amorphous Lithium Silicate Layer. *ACS Applied Energy Materials* **2020,** *3* (6), 5533-5541.

30. Park, K.; Yu, B.-C.; Jung, J.-W.; Li, Y.; Zhou, W.; Gao, H.; Son, S.; Goodenough, J. B., Electrochemical Nature of the Cathode Interface for a Solid-State Lithium-Ion Battery: Interface between $LiCoO_2$ and Garnet-$Li_7La_3Zr_2O_{12}$. *Chemistry of Materials* **2016,** *28* (21), 8051-8059.

Figure Legends

Figure 1. Chemical structure of organic-inorganic hybrid interfacial material.

Figure 2. a) Photos and illustration of the hybrid precursor solution containing $LiClO_4$ and derived membrane prepared by casting and subsequent heat treatment at 60 and 120 °C. b) Impedance profiles of hybrid solid electrolytes at room temperature (Information of fitting to equivalent circuit at S5a). c) Temperature dependence of the total lithium-ion conductivity of the hybrid solid electrolytes. d) and e) Cyclic voltammogram of hybrid solid electrolytes containing $LiClO_4$ at 25 °C and 60 °C. f) and g) Cyclic voltammogram of hybrid solid electrolytes containing LiTFSI at 25 °C and 60 °C.

Figure 3. a) Illustration of the fabrication of the all-solid-state battery by screen-printing of the composite electrode on the surface of LLCZT pellet. SEM images of b) $LiCoO_2$ particles, c)-d) surface of composite electrode containing hybrid solid electrolyte with $LiClO_4$ salt and e) cross-section of composite electrode and solid electrolyte interface. f) and g) Impedance profiles of as-prepared Li/LS/LLCZT/CE-hybrid ($LiClO_4$), Li/LS/LLCZT/LS/CE-hybrid ($LiClO_4$) and Li/LS/LLCZT/LS/CE-hybrid (LiTFSI) cells (Information of fitting to equivalent circuit at Figure S5b and S5c). h) and i) Initial charge-discharge curves of Li/LS/LLCZT/CE-hybrid ($LiClO_4$), Li/LS/LLCZT/LS/CE-hybrid ($LiClO_4$) and Li/LS/LLCZT/LS/CE-hybrid (LiTFSI) cells.

Figure 4. a) Illustration of the fabrication of the all-solid-state battery by using a composite electrode sheet obtained by doctor-blade method. b) Photos of the components of the all-solid-state battery before assembling. SEM images of surface and cross-section of composite electrode sheet with different particle size of $LiCoO_2$: c-d) 200 nm and e-f) 2 µm. Impedance profiles of as-prepared Li/LS/LLCZT/LS/CES-hybrid (LiTFSI) cells with g) small LCO and h) big LCO at room temperature (Information of fitting to equivalent circuit at Figure S5d). Initial charge-discharge profiles of Li/LS/LLCZT/LS/CES-hybrid (LiTFSI) cells with i) small LCO and j) big LCO at 25 °C.

Tables

Figure 1

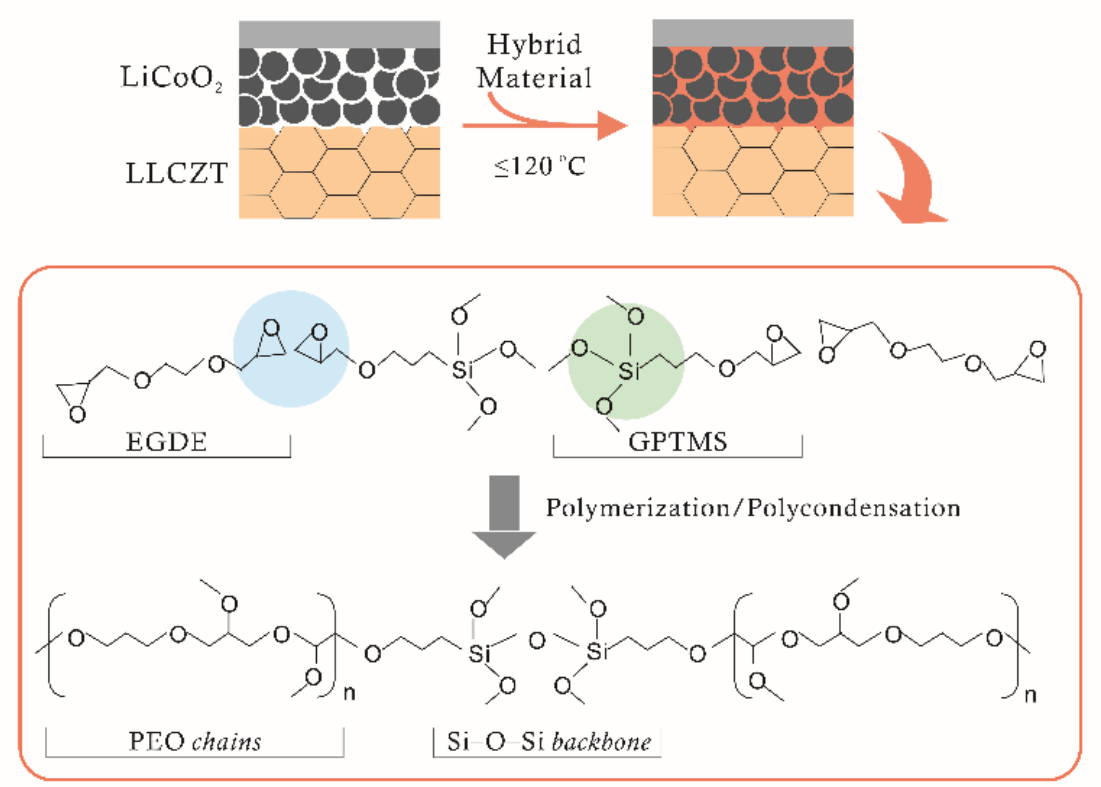

Figure 5. Chemical structure of organic-inorganic hybrid interfacial material.

Figure 2

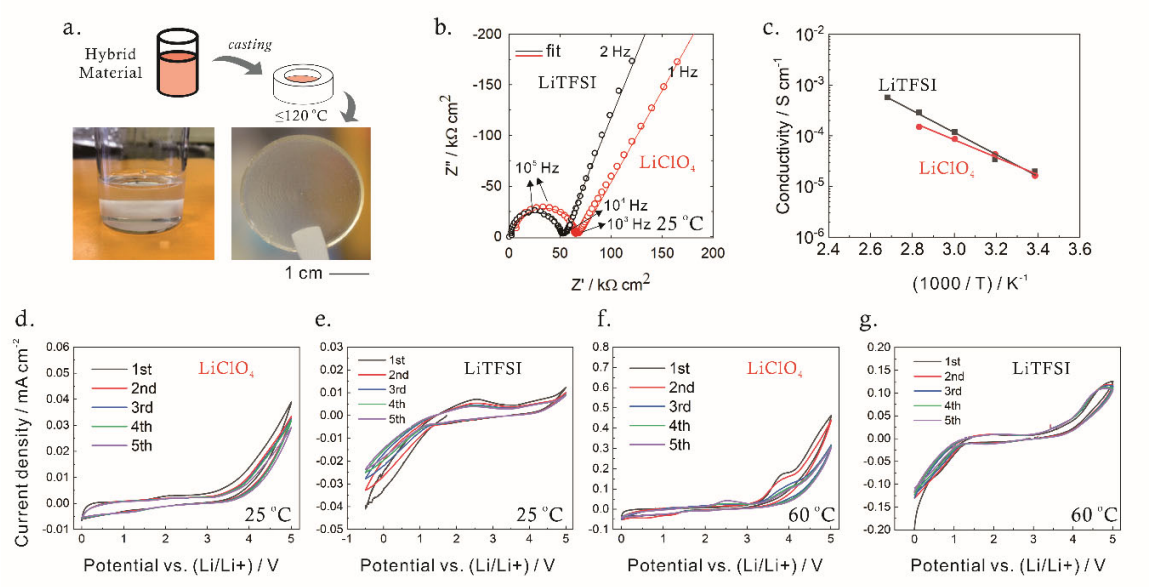

Figure 6. a) Photos and illustration of the hybrid precursor solution containing $LiClO_4$ and derived membrane prepared by casting and subsequent heat treatment at 60 and 120 °C. b) Impedance profiles of hybrid solid electrolytes at room temperature. c) Temperature dependence of the total lithium-ion conductivity of the hybrid solid electrolytes (Information of fitting to equivalent circuit at S5a). d) and e) Cyclic voltammogram of hybrid solid electrolytes containing $LiClO_4$ at 25 °C and 60 °C. f) and g) Cyclic voltammogram of hybrid solid electrolytes containing LiTFSI at 25 °C and 60 °C.

Figure 3

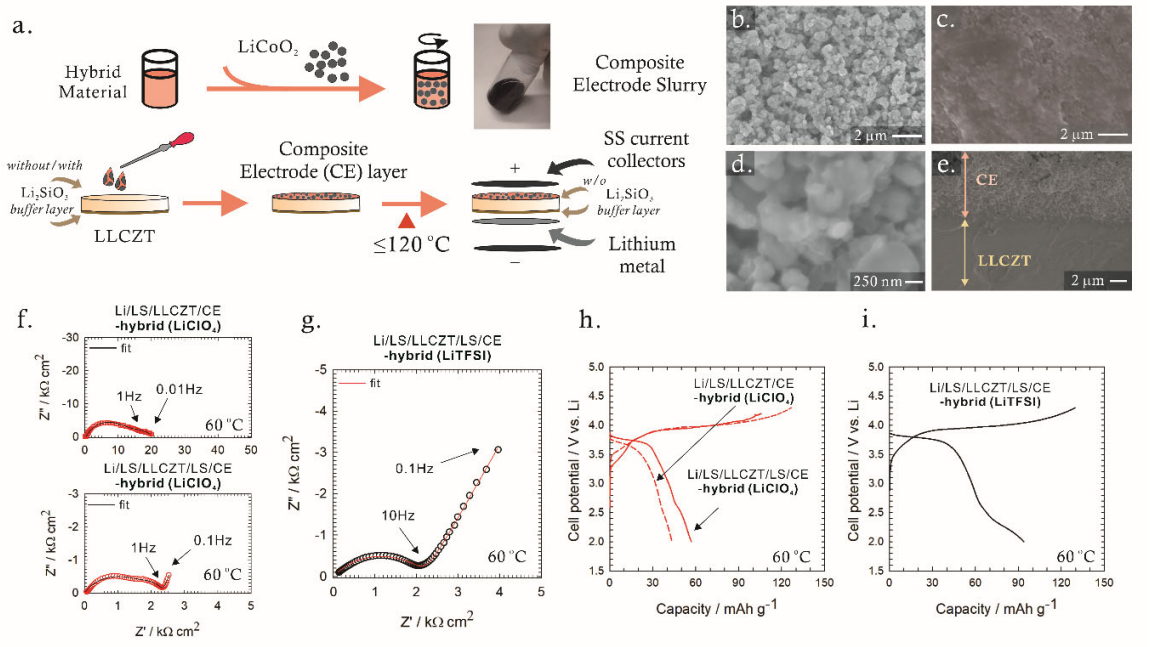

Figure 7. a) Illustration of the fabrication of the all-solid-state battery by screen-printing of the composite electrode on the surface of LLCZT pellet. SEM images of b) $LiCoO_2$ particles, c)-d) surface of composite electrode containing hybrid solid electrolyte with $LiClO_4$ salt and e) cross-section of composite electrode and solid electrolyte interface. f) and g) Impedance profiles of as-prepared Li/LS/LLCZT/CE-hybrid ($LiClO_4$), Li/LS/LLCZT/LS/CE-hybrid ($LiClO_4$) and Li/LS/LLCZT/LS/CE-hybrid (LiTFSI) cells (Information of fitting to equivalent circuit at Figure S5b and S5c). h) and i) Initial charge-discharge curves of Li/LS/LLCZT/CE-hybrid ($LiClO_4$), Li/LS/LLCZT/LS/CE-hybrid ($LiClO_4$) and Li/LS/LLCZT/LS/CE-hybrid (LiTFSI) cells.

Figure 4

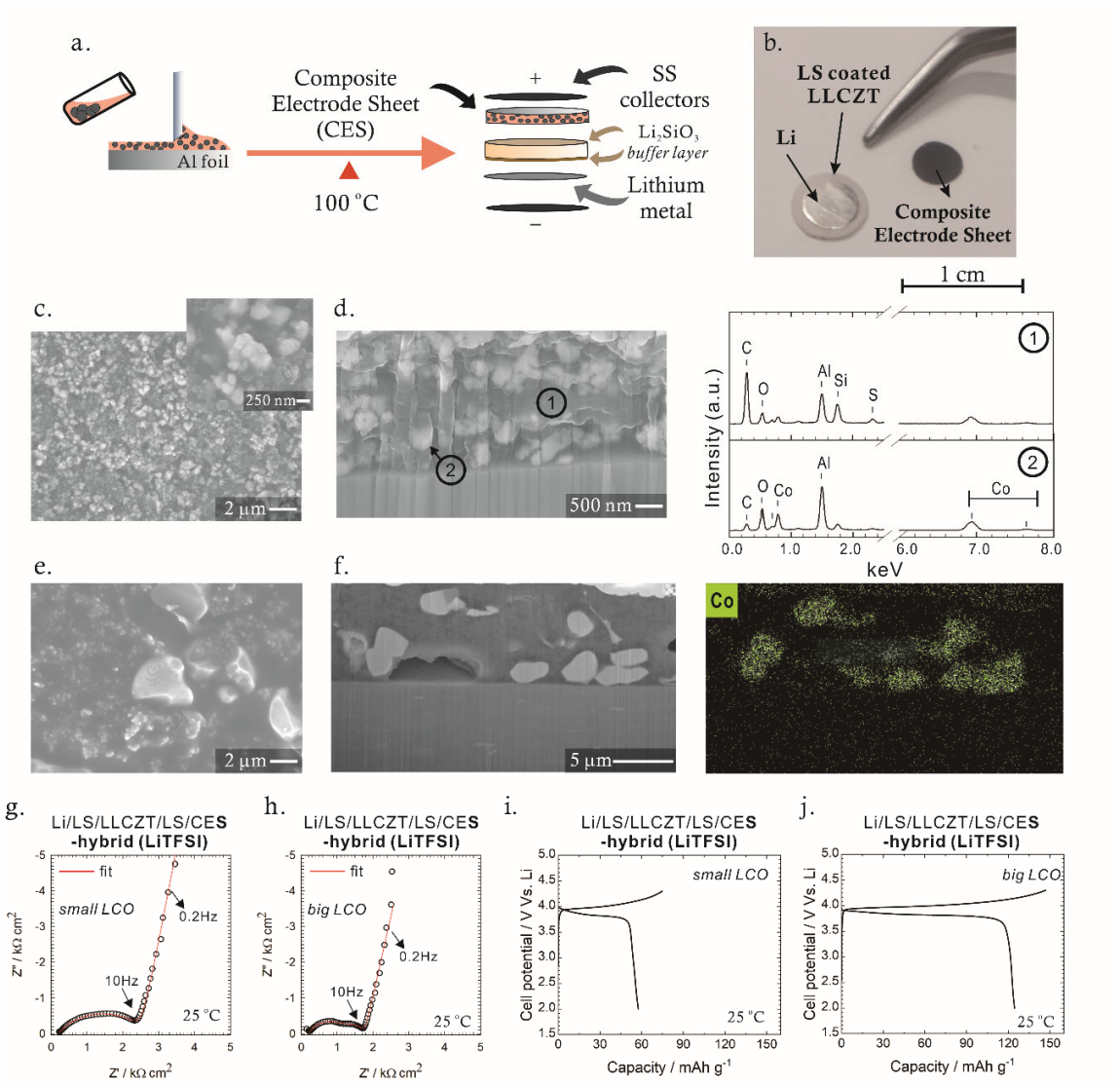

Figure 8. a) Illustration of the fabrication of the all-solid-state battery by using a composite electrode sheet obtained by doctor-blade method. b) Photos of the components of the all-solid-state battery before assembling. SEM images of surface and cross-section of composite electrode sheet with different particle size of $LiCoO_2$: c-d) 200 nm and e-f) 2 µm. Impedance profiles of as-prepared Li/LS/LLCZT/LS/CES-hybrid (LiTFSI) cells with g) small LCO and h) big LCO at room temperature (Information of fitting to equivalent circuit at Figure S5d). Initial charge-discharge profiles of Li/LS/LLCZT/LS/CES-hybrid (LiTFSI) cells with i) small LCO and j) big LCO at 25 °C.

Table I

Composite Electrode	All-solid-state batteries notation
screen-printing (Figure 3a)	Li/LS/LLCZT/CE-hybrid ($LiClO_4$)
	Li/LS/LLCZT/LS/CE-hybrid ($LiClO_4$)
	Li/LS/LLCZT/LS/CE-hybrid (LiTFSI)
sheet by doctor-blade (Figure 4a)	Li/LS/LLCZT/LS/CES-hybrid (LiTFSI)

Abbreviations. CE: composite electrode by screen-printing on the modified or unmodified LS surface of LLCZT pellet; CES: composite electrode sheet obtained by doctor-blade method on aluminum foil; LS: lithium silicate buffer layer. The CEs were prepared with a particle size of $LiCoO_2$ of ~200 nm while CESs were prepared with two different particle sizes of $LiCoO_2$ of ~200 nm (small LCO) and ~2 μm (big LCO).

Table II

Year	Cathode	Process / Temperature		Capacity ($mAh.g^{-1}$)	c-rate or current density ($\mu A.cm^{-2}$)	Battery temperature	REF
Solid-solid interfaces using ceramic interfaces							
2010	$LiCoO_2$	Co-sintering (*in-situ* deposition)	800 ºC	0.015	2	NS	[8]
2011	$LiCoO_2$	PLD	-	125	3.5	25 ºC	[3]
2012	$LiCoO_2$	PLD	-	130	3.5	100 ºC	[4]
2013	$LiCoO_2$	Screen-printing	700 ºC	85	10	25 ºC	[9]
2014	$LiCoO_2$	PLD	-	80	1	NS	[6]
2014	$LiCoO_2$	Co-sintering	800 ºC	78	0.01C	NS	[7]
2016	$LiCoO_2$	Screen-printing	700 ºC	101	5	25 ºC	[10]
2018	$LiCoO_2$	Screen-printing	700 ºC	94	10	25 ºC	[12]
2018	NMC	Screen-printing	300 ºC	138	10	100 ºC	[13]
2013	$Cu_{0.1}V_2O_5$	Screen-printing	120 ºC	53	5	25 ºC	[11]
2016	TiS_4	PLD	-	500	10	25 ºC	[5]
Solid-solid interfaces using polymers							
2015	$LiFePO_4$	Screen-printing	80 ºC	126	0.05C	60 ºC	[14]
2019	$LiFePO_4$	Sheet*	50 ºC	135	0.2 C	90 ºC	[15]
New solid-solid interface using hybrid solid electrolyte							
2020	$LiCoO_2$	Sheet*	100 ºC	125	5.5	25 ºC	This work

Abbreviations. NMC: $LiNi_{1/3}Mn_{1/3}Co_{1/3}O_2$, NS; non-specified. *Refers to composite electrode sheet obtained by doctor-blade process and put on the surface of the solid electrolyte.